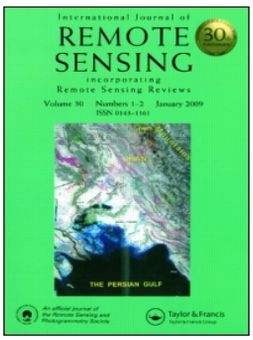

International Journal of Remote Sensing

ISSN: 0143-1161 (Print) 1366-5901 (Online) Journal homepage: https://www.tandfonline.com/loi/tres20

In situ validation of MERIS marine reflectance off the southwest Iberian Peninsula: assessment of vicarious adjustment and corrections for near-land adjacency

Sónia Cláudia Vitorino Cristina, Gerald Francis Moore, Priscila Raquel Fernandes Costa Goela, John David Icely & Alice Newton

To cite this article: Sónia Cláudia Vitorino Cristina, Gerald Francis Moore, Priscila Raquel Fernandes Costa Goela, John David Icely & Alice Newton (2014) *In situ* validation of MERIS marine reflectance off the southwest Iberian Peninsula: assessment of vicarious adjustment and corrections for near-land adjacency, International Journal of Remote Sensing, 35:6, 2347-2377, DOI: 10.1080/01431161.2014.894657

To link to this article: https://doi.org/10.1080/01431161.2014.894657

Published online: 07 Mar 2014.

International Journal of Remote Sensing, 2014
Vol. 35, No. 6, 2347–2377, http://dx.doi.org/10.1080/01431161.2014.894657

Taylor & Francis
Taylor & Francis Group

In situ validation of MERIS marine reflectance off the southwest Iberian Peninsula: assessment of vicarious adjustment and corrections for near-land adjacency

Sónia Cláudia Vitorino Cristina[a,b]*, Gerald Francis Moore[c], Priscila Raquel Fernandes Costa Goela[a,b], John David Icely[a,d], and Alice Newton[a,e]

[a]*CIMA-FCT, University of Algarve, Faro, Portugal;* [b]*Facultad de Ciencias del Mar y Ambientales, University of Cadiz, Puerto Real, Cadiz, Spain;* [c]*Bio-Optika, Crofters, Gunnislake, UK;* [d]*Sagremarisco Lda., Vila do Bispo, Portugal;* [e]*NILU-IMPEC, Kjeller, Norway*

(*Received 8 June 2013; accepted 18 December 2013*)

Water-leaving reflectance (ρ_w) data from the European Space Agency ocean colour sensor Medium Resolution Imaging Spectrometer (MERIS) was validated with *in situ* ρ_w between October 2008 and November 2011, off Sagres on the southwest coast of the Iberian Peninsula. The study area is exceptional, since Stations A, B, and C at 2, 10, and 18 km offshore are in optically deep waters at approximately 40, 100, and 160 m, respectively. These stations showed consistently similar bio-optical properties, characteristic of Case 1 waters, enabling the evaluation of adjacency effects independent of the usual co-varying inputs of coastal waters. Using the third reprocessing of MERIS with the standard MEGS 8.1 processor, four different combinations of procedures were tested to improve the calibration between MERIS products and *in situ* data. These combinations included no vicarious adjustment (NoVIC), vicarious adjustment (VIC), and, for mitigating the effects of land adjacency on MERIS ρ_w, the improved contrast between ocean and land (ICOL) processor (version 2.7.4) and VIC + ICOL. Out of approximately 130 potential matchups for each station, 38–77%, 74–86%, and 88–90% were achieved at Stations A, B, and C, respectively, depending on which of the four combinations were used. Analyses of ρ_w comparing these various procedures, including statistics, scatter plots, histograms, and MERIS full-resolution images, showed that the VIC procedure compared with NoVIC produced minimal changes to the calibration. For example, at the oceanic Station C, the regression slope was closer to unity at all wavelengths with NoVIC compared to VIC, whereas, with the exception of wavelengths 412 and 443 nm, the intercept, mean ratio (MR), absolute percentage difference (APD), and relative percentage difference (RPD) were better with NoVIC. The differences for MR and APD indicate that there was marginal improvement for these two bands with VIC, and an over-adjustment with RPD. ICOL also showed inconsistent results for improving the retrieval of the near-shore conditions, but under some conditions, such as ρ_w at wavelength 560 nm, the improvement was striking. VIC + ICOL showed results intermediate between those of VIC and ICOL implemented separately. In relation to other validation sites, the offshore Station C at Sagres had much in common with the Mediterranean deep water, BOUSSOLE buoy, although the matchup statistics between MERIS ρ_w and *in situ* ρ_w were much better for Sagres than for BOUSSOLE. Strikingly, the matchup statistics for ρ_w at Sagres were very similar to those for the Acqua Alta Oceanographic Tower (AAOT), where the AAOT showed more scatter at 412 nm, probably because of the atmospheric correction where the aerosol optical thickness is higher at the AAOT.

*Corresponding author. Email: cristina.scv@gmail.com

Conversely, Sagres showed much greater scatter at 665 nm in the red as the values were generally close to the limits of detection owing to the clearer waters at Sagres compared to the more turbid waters at the AAOT.

1. Introduction

It is essential to understand oceanic and coastal processes in an era of global change partly driven by human activities (Newton and Icely 2008), and it is probable that only through remote sensing of key drivers, such as wind conditions, sea surface temperature, and primary production, that the necessary temporal and spatial data can be obtained to achieve this understanding. For example, remote sensing of ocean colour over the last 30 years (Platt et al. 2008) has provided synoptic information on primary production (Behrenfeld et al. 2006; Field et al. 1998), detection of algal blooms (Ahn and Shanmugam 2006; Carvalho et al. 2011), physical oceanography (McClain et al. 2002), fisheries biology (Santos 2000), sediment transport (Eleveld et al. 2008), and coastal management (Banks et al. 2012; Platt and Sathyendranath 2008).

Considering the diversity of applications for remote-sensing data, it is important that satellite products are accurate and that they can be compared between different sensors. Combining internal calibration procedures for the satellite sensors with vicarious calibration, based on *in situ* measurements, provides a useful approach for checking the accuracy of remote-sensing products (Morel 1998). This calibration is a continuous programme during the lifetime of a sensor for analysing field data together with instrument parameters to obtain values for the uncertainties of the derived satellite products (Antoine, d'Ortenzio, et al. 2008; McClain et al. 1992). In the specific case of ocean colour, this approach was developed by the Ocean Biology Processing Group (OPBG) for the National Aeronautics and Space Administration (NASA), since the launch of the proof-of-concept Coastal Zone Scanner (CZCS) by NASA and their subsequent colour sensors including the Sea-viewing Wide Field-of-view Sensor (SeaWiFS) and the Moderate Resolution Spectroradiometer (MODIS) (Bailey and Werdell 2006). Essentially, the integrated instrument and atmospheric correction system are adjusted to retrieve normalized water leaving radiances that are in agreement with *in situ* measurements (Bailey and Werdell 2006; Antoine, d'Ortenzio, et al. 2008; Franz et al. 2007). These comparative measurements are subsequently stored in databases such as the SeaWiFS Bio-optical Archive and Storage System (SeaBASS) (Hooker et al. 1994).

In the case of the Medium Resolution Imaging Spectrometer (MERIS), which is the ocean colour sensor launched on the ENVISAT satellite by the European Space Agency (ESA), vicarious calibration was initially not considered necessary due to the rigorous characterization of the sensor before its launch, and the improvement of the on-board calibration systems compared to other missions (Antoine, d'Ortenzio, et al. 2008). However, this opinion has altered in recent years to the view that vicarious calibration should be used for MERIS (Kwiatkowska et al. 2008; McCulloch, Barker, and Zibordi 2010; Zibordi, Mélin, and Berthon 2006).

The validation activities for these ocean colour sensors are based on long-term calibration reference stations, which include the Marine Optical Bouy (MOBY; Broenkow, Clark, and Yarbrough 1996) off Hawaii in the Pacific Ocean, the Acqua Alta Oceanographic Tower (AAOT; Zibordi et al. 2002, Zibordi, Mélin, and Berthon 2006; Zibordi et al. 2013) in the Adriatic Sea, and the Bouée pour l'acquisition de Séries Optiques à Long Terme (BOUSSOLE; Antoine, Guevel, et al. 2008) off Nice in the Mediterranean. However, these reference stations have limited geographical coverage and

there are regional differences for optical characteristics (Dowell and Platt 2009) throughout the oceans (Longhurst 1998, 2006). Therefore, it is important to have validation activities covering other regions. Using MERIS as an example, there are additional validation sites from the Baltic Sea (Kratzer, Brockmann, and Moore 2008), the Skagerrak (Sørensen, Aas, and Høkedal 2007), the North Sea (Petersen et al. 2008; Ruddick et al. 2008), and areas outside Europe, such as China (Cui et al. 2010).

A recent addition to these sites is Sagres along the southwest coast of the Iberian Peninsula (Figure 1). The locations of the *in situ* stations selected for validation measurements are at 2, 10, and 18 km offshore and at respective depths of 40, 100, and 160 m along a north to south transect (37° 00′ 34″ N; 8° 54′ 07″ W), perpendicular to the coast off Sagres (A, B, and C in the inset of Figure 1). Station C has been selected as a validation site because of its potential to achieve a high frequency of measurements close in time between *in situ* stations and satellites, commonly called matchups. Furthermore, in terms of location and adjacency contamination, Station C has many similarities to the Venice AAOT, although in contrast to the Sagres site, the Venice AAOT is only at a depth of 17 m and is bio-optically more complex (Zibordi et al. 2009). Closer to the shore at Sagres, Stations A and B have been added specifically to address adjacency contamination. Zibordi et al. (2009) suggest from a theoretical analysis that observations between 9 and 18 km might be suitable for validation studies despite potential perturbations from adjacency effects on the satellite products. Indeed, they also suggest that *in situ* measurements close to the coast are valuable for supporting studies on minimizing these adjacency effects.

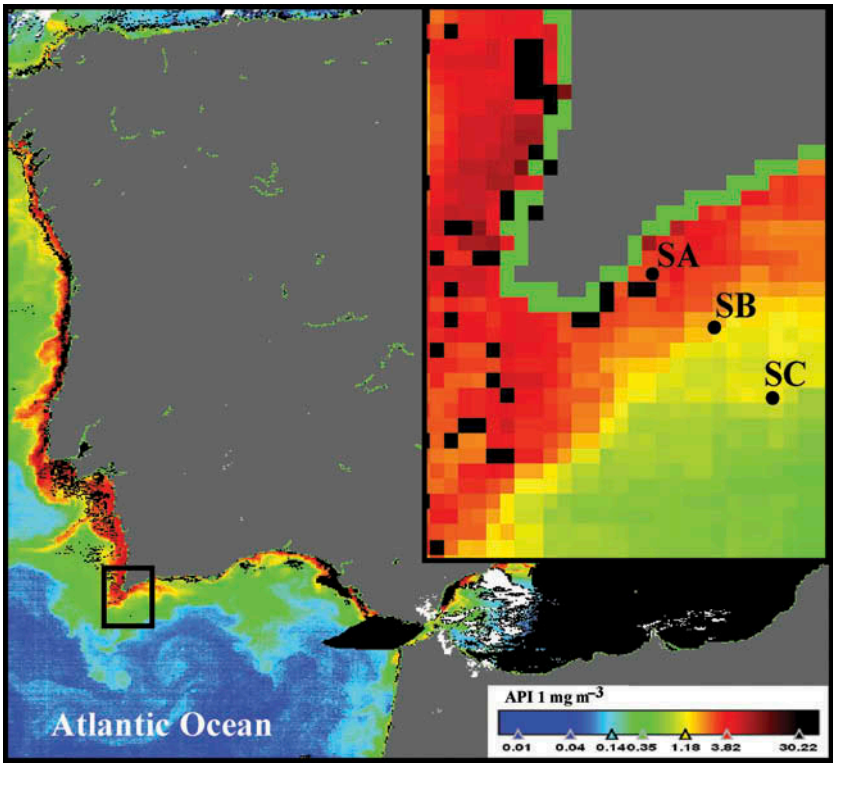

Figure 1. Satellite image of MERIS algal pigment index 1 (API 1) for the southwest coast of Portugal with the inset showing locations of Stations A (37° 00′ 39″ N and 8° 53′ 58″ W), B (36° 56′ 06″ N and 8° 52′ 48″ W), and C (36° 51′ 33″ N and 8° 50′ 16″ W) off the peninsula at Sagres.

The validation work at Sagres is focused on the MERIS sensor, which had been operational since the launch of ENVISAT in 2002 (Rast, Bezy, and Bruzzi 1999) until contact was lost with the satellite in April 2012. This sensor provided spectral information in 15 bands from 412 to 890 nm, with reduced spatial resolution (RR) at 1200 m and full spatial resolution (FR) at 300 m. A preliminary validation of MERIS with *in situ* water-leaving reflectances (ρ_w) from Sagres was reported by Cristina et al. (2009), where five days of matchups were achieved during the last six months of 2008. Their study concludes that there is a wide scatter in the data, especially at the blue wavelengths, and that the satellite-derived marine reflectance near the coast is underestimated due to error in the atmospheric correction caused by Rayleigh and aerosol scattering from the nearby land surface (Santer 2010).

In this current study, matchup data for *in situ* and MERIS ρ_w from the standard MERIS processor MEGS 8.1 will be compared to test the efficacy of different combinations in the processing chain for all the viewing and oceanic conditions at Sagres. These combinations include no vicarious adjustment (NoVIC) and vicarious adjustment (VIC); we use the term vicarious adjustment, rather than vicarious calibration, as Lerebourg et al. (2011) use VIC to adjust internally the Level 2 Ocean branch processing and not to modify the Level 1 top of atmosphere (TOA) radiometric calibration. The VIC procedure adopted for MERIS (Lerebourg et al. 2011) follows a methodology similar to that of Franz et al. (2007), using data from the South Pacific gyre and Southern Indian Ocean for calibration in the near infrared (NIR) and using data from MOBY, and additional clear-water validation sites for the calibration at visible wavelengths. The adjustment is applied to TOA reflectances that are calibrated and corrected for glint. The bands 709 and 779 nm in the NIR are used for reference, whereas coefficients are used to derive the remaining NIR bands. The greatest differences between the reference and the derived bands occur at 865 and 885 nm (Figure 2). Lerebourg et al. (2011) ascribe these changes to possible residual stray light in the sensor; however, errors in glint correction may be an alternative explanation. The coefficients for the visible wavelengths are derived using the entire processing chain and tend to show a stronger effect in the blue wavelength. The net effect of these changes is to bring the radiometry closer to the 1:1 relationship for clear-water

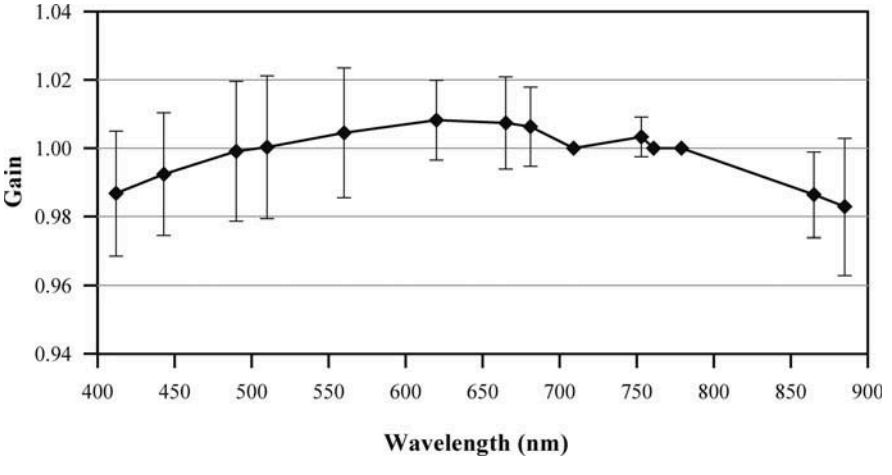

Figure 2. Gain spectra at 95% confidence limits for MERIS third reprocessing used for VIC (adapted from Lerebourg et al. (2011)).

sites (MQWG 2012). There are, however, concerns about the adjustment, since there are offsets in the mean monthly remote-sensing reflectance (R_{rs}) ratios for MODIS and SeaWiFS (MQWG 2012), and because there is a reduction in valid matchups compared to the second reprocessing (MQWG 2011). It is also important to note that most of the differences between these coefficients at different wavelengths are not statistically significant at the 95% confidence level (Figure 2).

An additional combination to the MERIS processing chain is the Improved Contrast between Ocean and Land (ICOL) processor, which has been implemented to correct for adjacency effects. These have been extensively studied by Santer and Schmechtig (2000), using 5S model calculations to demonstrate that the influence of adjacency is the strongest close to shore but can still be significant up to 20 km offshore, depending on the relative contributions of Rayleigh and aerosol scattering. Where Raleigh scattering dominates, the effects are seen further offshore owing to the higher scale height of Rayleigh scattering compared to that of aerosol scattering. This effect should be corrected by ICOL (Santer 2010; Santer and Zagolski 2009), which computes the TOA signal by removing the signal from the adjacent land pixels, thereby providing a product that can be used in ocean colour processors. Since VIC is also applied to the entire processing chain, and ICOL substantially changes the processing in near-shore waters, the effect of ICOL is tested in this study both without vicarious adjustment (ICOL) and with vicarious adjustment (VIC + ICOL).

The development of good-quality remote-sensing products for monitoring these waters, particularly near the coast, would have important economic benefits for this region, where there is commercial fishing, a rapidly expanding aquaculture industry, and tourism based on cetacean and bird watching, recreational fishing, diving, and surfing (Loureiro, Newton, and Icely 2005, Loureiro et al. 2011).

2. Study area

2.1. General description

The coast at Sagres has a characteristic narrow continental shelf that descends rapidly to depths of over 1000 m at the continental slope. As the summer months are dominated by northerly winds, an offshore Ekman transport drives an upwelling of relatively cool, nutrient-rich, subsurface waters along the west coast; after a prolonged period of northerly winds, upwelled waters will circulate around Cape Saint Vincent at the southwestern tip of the Iberian Peninsula and flow eastwards along the southern shelf, including the Sagres area (Loureiro, Newton, and Icely 2005; Relvas and Barton 2005; Relvas et al. 2007). These changes in water masses induce variations in the productivity and the bio-optical properties of the waters around Sagres. Although the subject of this article is radiometric reflectances, the bio-optical properties should be known for Sagres to facilitate the interpretation of radiometric measurements.

2.2. Bio-optical properties

During the deployment of the radiometer, water samples were taken using a Niskin bottle at three depths (0 m, ½ Secchi depth, and 1 Secchi depth). The processing of these samples and subsequent chemical analysis are described in more detail in Cristina et al. (2010) and Goela et al. (2013). The water samples were essentially treated to obtain *in situ* values for standard MERIS products including: algal pigment index 1 (API 1)

Table 1. Statistics for the bio-optical properties at Stations A, B, and C. Spectral diffuse attenuation coefficient at 490 nm ($K_d(490)$); algal pigment index 1 – total chlorophyll *a* and its degradation products (API 1); total suspended matter (TSM); absorption coefficient at 443 nm for phytoplankton (a_{ph}); absorption coefficient at 443 nm for non-algal particles (a_{nap}); and absorption coefficient at 443 nm for yellow substance (a_{ys}).

		Station A	Station B	Station C
Depth	Average ± SD	41.1 ± 7.0	104.4 ± 3.3	160.3 ± 40.5
(m)	Min. – Max.	32.3–57.0	96.0–109.0	103.0–242.0
Transparency	Average ± SD	11.0 ± 2.8	14.6 ± 5.7	16.5 ± 6.1
(m^{-1})	Min. – Max.	7.0–16.5	7.0–29.0	7.0–31.0
$K_d(490)$	Average ± SD	0.13 ± 0.05	0.09 ± 0.05	0.08 ± 0.04
(m^{-1})	Min. – Max.	0.06–0.25	0.04–0.22	0.03–0.18
API 1	Average ± SD	0.91 ± 0.63	0.71 ± 0.54	0.50 ± 0.34
(mg m^{-3})	Min. – Max.	0.10–2.27	0.09–2.10	0.08–1.17
TSM	Average ± SD	1.87 ± 0.61	1.79 ± 0.61	1.76 ± 0.63
(ug.$^{-1}$)	Min. – Max.	0.80–3.00	0.70–2.90	0.45–2.80
a_{ph} (443)	Average ± SD	0.06 ± 0.03	0.05 ± 0.04	0.04 ± 0.03
(m^{-1})	Min. – Max.	0.01–0.12	0.01–0.15	0.01–0.13
	Total % (Average ± SD)	48.4 ± 16.5	45.4 ± 20.3	46.8 ± 21.5
a_{nap} (443)	Average ± SD	0.01 ± 0.01	0.01 ± 0.01	0.00 ± 0.00
(m^{-1})	Min. – Max.	0.00–0.03	0.00–0.04	0.00–0.02
	Total % (Average ± SD)	8.8 ± 6.6	8.8 ± 9.5	6.4 ± 7.4
a_{ys} (443)	Average ± SD	0.05 ± 0.03	0.06 ± 0.04	0.04 ± 0.03
(m^{-1})	Min. – Max.	0.01–0.12	0.01–0.16	0.00–0.11
	Total % (Average ± SD)	42.8 ± 18.4	45.8 ± 21.1	46.8 ± 22.4

corresponding to the total concentration of chlorophyll *a* and its degradation products; algal pigment index 2 (API 2) corresponding to only chlorophyll *a* concentration; and total suspended matter (TSM). The statistics for these variables are shown in Table 1 and also include the following: water transparency; the spectral diffuse attenuation coefficient, $K_d(490)$; and the absorption coefficients at 443 nm for phytoplankton (a_{ph}), non-algal particles (a_{nap}), and yellow substance (a_{ys}). All three stations are characterized by low turbidity, with mean Secchi depths of between 11.0 and 16.5 m. The means of the $K_d(490)$ range between 0.08 and 0.13 m^{-1}, with minimum and maximum values of 0.03 and 0.25 m^{-1}, and relate to the means for API 1 of between 0.08 and 2.27 mg m^{-3}. The three stations tend to show increasing productivity towards the shore with mean API 1 increasing from 0.50 mg m^{-3} at Station C to 0.91 mg m^{-3} at Station A. Log $K_d(490)$ is correlated with log API 1, with a coefficient of determination (R^2) of 68.2%. This relationship can be expressed as in Equation (1):

$$K_d(490) = \chi(490)[\mathrm{Chl}]^{e(490)} + K_w(490), \quad (1)$$

where [Chl] is defined identically as API 1 (Morel and Antoine 1994; Morel and Maritorena 2001), with values $\chi = 0.072$ and $e = 0.689$ (Morel and Maritorena 2001), and K_w is the diffuse attenuation coefficient for pure water. In this study, $\chi = 0.094 \pm 0.009$ and $e = 0.654 \pm 0.102$, where the value of χ is significantly higher, indicating that the $K_d(490)$ is slightly lower than expected for a given pigment value, and e is not significantly different from the Morel and Maritorena value. However, the values for Sagres are based on a much lower sample number and dynamic range than from the Morel and Maritorena study and, as such, are subject to outliers. The $K_d(490)$ *versus* [Chl]

relationship is comparable with the Gordon and Morel (1983) definition of Case 1 *versus* Case 2 waters.

The absorption coefficients at 443 nm for a_{ph}, a_{nap}, and a_{ys} are presented in Figure 3 using the ternary diagrams classification proposed by Prieur and Sathyendranath (1981). In general, the properties at the three stations at Sagres are similar over an individual sampling campaign. Furthermore, the percentage differences between a_{ph}, a_{nap}, and a_{ys} are, respectively, 48, 9, and 43 for Station A and 47, 6, and 47 for Station C (Table 1), confirming that there are only limited differences between the coastal and offshore stations, and that these Case 1 waters are dominated by phytoplankton and yellow substances. The proportion of a_{ys} is comparable with that in the NOMAD database (Werdell and Bailey 2005), where the value is 42.2 ± 17.2.

3. Data and methods

The validation campaigns for this study at Sagres have taken into account the seven key recommendations by Bailey and Werdell (2006) for the validation of ocean colour sensors: (1) use a consistently processed *in situ* data set; (2) eliminate suspect *in situ* data (e.g. from optically shallow waters) from the validation set; (3) use a narrow time window for determining coincidence (i.e. no more than ±3 h) between *in situ* and satellite data records; (4) use native resolution satellite products (i.e. avoid sub-sampled data); (5) use the mean of a 5 × 5 pixel box centred on the *in situ* location; (6) mask satellite pixels appropriately on the Level 2 flags; and (7) use a homogeneity test to minimize the impact of geophysical variability in the 5 × 5 pixel box on the mean of satellite measurements.

The measurements for radiometric, atmospheric, and water variables in this study are consistent with the protocols for the validation of MERIS products (Barker 2011 see: http://hermes.acri.fr/mermaid/dataproto/CO-SCI-ARG-TN-0008_MERIS_Optical_Measurement_Protocols_Issue2_Aug2011.pdf, and Doerffer, 2002 see: https://earth.esa.int/workshops/mavt_2003/MAVT-2003_801_MERIS-protocols_issue1.3.5.pdf).

3.1. In situ *radiometric data*

In situ radiometric measurements were collected between October 2008 and November 2011 from Stations A, B, and C. The radiometer used for these measurements was a tethered attenuation coefficient chain sensor (TACCS) manufactured by Satlantic Inc., Halifax, NS, Canada, comprising a floating buoy encasing a hyperspectral surface irradiance sensor $E_s(\lambda)$ and a subsurface radiance sensor $L_u(\lambda)$ located 0.62 m below the surface, as well as a tethered attenuation chain (K-chain) supporting four subsurface irradiance sensors $E_d(z)$ attached at nominal depths (z) of 2, 4, 8, and 16 m. Initially, $E_d(z)$ was measured only at 490 nm, but after an upgrade in 2010, $E_d(z)$ was also measured at 412, 560, and 665 nm. A compass with a pitch and roll sensor was also incorporated in the TACCS during the upgrade of the sensors. The small size of the TACCS and the flexible attenuation chain allowed rapid deployment of the instrument from small boats for responsive sampling during campaigns for satellite matchups (Moore, Icely, and Kratzer 2010).

The *in situ* measurements were timed to coincide with the MERIS overpass within ±30 minutes at Station A and within ±1.5 hours at Stations B and C. At each site, the TACCS was deployed up to 20 m clear of the boat to avoid interference to the light pattern from the shadow of the boat. After a period of acclimatization to the water temperature, the instrument recorded five sets of data, each for 2 min, at a rate of

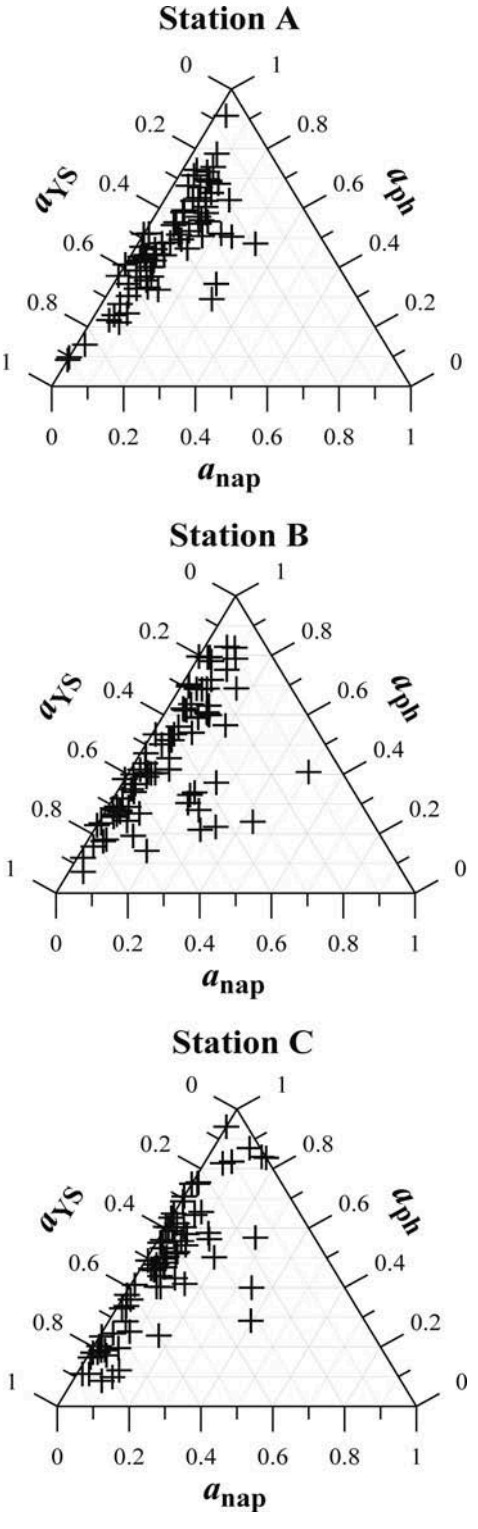

Figure 3. Ternary diagram for Stations A, B, and C showing the relative contribution of absorption coefficients at 443 nm for the absorption by phytoplankton (a_{ph}), the absorption by non-algal particles (a_{nap}), and the absorption by yellow substance (a_{ys}). Each measurement is represented by (+).

approximately one sample per second (depending on the integration time). The hyper-spectral sensors have shutters that provide dark readings at the same integration time as the light readings, approximately every three seconds. These data were interpolated to provide the dark offset for the spectra between wavelengths (λ) of 350 and 800 nm. For the $E_d(z)$ sensors, dark readings were taken immediately post-deployment so that temperature effects were minimized.

The location and meteorological data at each sampling site were recorded continuously during the deployment of the radiometer with an Airmar PB150 ultrasonic weather station (Milford, NH, USA). At each station, the atmospheric conditions were also recorded with a MICROTOPS II sunphotometer (version 5.5; Solar Light Company Inc., Glenside, PA, USA) to provide data on atmospheric pressure, water vapour, and aerosol optical thickness (AOT) at the wavelengths 380, 500, 870, 936, and 1020 nm. Activities related to water variables have been introduced in Section 2.2.

3.2. *Processing* in situ *radiometric data*

The raw data from each sensor were converted from binary to calibrated engineering units using Satlantic SatCon software that could then be visually screened for stability over each cast and rejected if there were excessive noise artefacts. Since the spectrographs had slightly different spectral sampling points, the two hyper-spectral sensors were co-aligned by linear interpolation to a 1 nm grid. The data from the sensors of $E_s(\lambda)$, $L_u(\lambda)$, and $E_d(z)$ were corrected for the dark signal. The spectral diffuse attenuation coefficient K_d (m^{-1}) from multi-depth $E_d(z)$ at 412, 490, 560, and 665 nm was determined from the slope for the natural log regression of the K-chain. E_d was obtained from the intercept at 412, 490, 560, and 665 nm for measurements at each depth except for 2008 and 2009 data, where only data at 490 nm was available. For the 2010 and 2011 data, the K_d for the other wavelengths was estimated by first determining $K_d'(490)$ as in Equation (2):

$$K_d'(490) = K_d(490) - K_w(490), \tag{2}$$

where $K_w(490)$ is taken from Morel and Antoine (1994).

Second, K_d' was determined at other wavelengths by converting the $K_d'(490)$ obtained from Equation (2) into the apparent chlorophyll using a simple inversion from Equation (3), again using the coefficients of Morel and Antoine (1994):

$$K_d'(\lambda, \mathrm{Chl}) = \chi(\lambda)\,[\mathrm{Chl}]^{e(\lambda)}. \tag{3}$$

$K_d(\lambda)$ was then estimated as in Equation (4):

$$K_d(\lambda) = K_d'(\lambda) + K_w(\lambda), \tag{4}$$

where the K_d spectra derived from the chlorophyll were normalized to K_d at 412, 490, 560, and 665 nm, so that the final spectra were correct at the measured wavelengths.

The upwelling radiance L_u was extrapolated to just below the sea surface as in Equation (5):

$$L_u(0^-, \lambda) = \frac{L_u(\lambda)}{e^{-0.62\,K_L(\lambda)}}, \tag{5}$$

where $K_d(\lambda)$ obtained from Equation (4) is assumed to approximate to $K_L(\lambda)$ in Equation (5). The assumption that K_d is a good estimate of K_L has been tested using a simulated dataset calculated with Hydrolight (Mobley 1995) for both Case 1 and Case 2 waters. For these data, a realistic range of absorption (a) and scattering (b) is generated with an increasing single scattering albedo ranging from that of pure water to 0.6. K_d is then calculated at the K-chain depths from the simulated data using the log linear regression. K_L is determined from the upwelling radiance at the depth of the radiance sensor, and that just below the surface. From these runs of the model, the mean value of the ratio between K_d and K_L was 1.005, but this has a scatter dependent on the single scattering albedo of ±0.02. This additional uncertainty of 1–2% in the extrapolation of the measured radiance to the surface is accounted for in the error budget given in Table 2. The factor 0.62 is the depth offset for the $L_u(\lambda)$ sensor. From $L_u(0^-,\lambda)$, the water leaving radiance $L_w(\lambda)$ was determined as in Equation (6):

$$L_w(\lambda) = L_u(0^-,\lambda)\frac{(1-\rho)}{n_w^2}, \tag{6}$$

where n_w is the refractive index of seawater and ρ is the air sea surface reflectance from below, which depends on wind speed and view angle. The term $(1-\rho)/n_w^2$ is the upward radiance transmittance of the sea surface for normal incidence from below and is approximately 0.54, with the exact values for nadir viewing in seawater taken from Table 10-1 in Barker (2011).

The E_s data between 2010 and 2011 were calculated by two methods depending on whether the minimum pitch and roll during the sampling period was close to zero. If the minimum pitch and roll minimum were close to zero (<2°), then the E_s value was taken at the time when the TACCS was the closest to vertical. Where the minimum pitch and roll was not close to vertical, then a correction was performed under the assumption that the diffuse solar irradiance was isotropic, and that the direct irradiance could be corrected by calculating the angle with the cosine collector.

First, the ratio of direct to total irradiance (d_t) was estimated from Equation (7):

$$d_t = \frac{E_{dir}}{E_{tot}}. \tag{7}$$

Table 2. Summary of the uncertainty budget for water-leaving reflectance (ρ_w) determined for the TACCS at Station A (SA), Station B (SB), and Station C (SC) for wavelengths 443, 490, and 560 nm.

	443 nm			490 nm			560 nm		
Uncertainty source	SA	SB	SC	SA	SB	SC	SA	SB	SC
Absolute calibration of $L_u(\lambda)$	2.8	2.8	2.8	2.8	2.8	2.8	2.8	2.8	2.8
Self-shading corrections	0.7	0.7	0.7	0.7	0.7	0.7	0.7	0.7	0.7
Absolute calibration of $E_d(\lambda)$	3.1	3.1	3.1	3.1	3.1	3.1	3.1	3.1	3.1
Bio-optical assumptions	2.2	2.2	2.2	1.2	1.2	1.2	2.0	2.0	2.0
Geometrical effects	4.5	4.5	4.5	4.5	4.5	4.5	4.0	4.0	4.0
Environmental perturbations	2.8	3.0	3.8	3.1	3.2	5.0	4.0	3.5	4.6
Quadrature sum (%)	7.1	7.2	7.6	7.0	7.1	8.1	7.4	7.1	7.7

Second, the angle of the solar angle (θ_{sun}), and the apparent angle of the sun to the irradiance sensor (θ_{sen}), was calculated. The correction factor f for the direct irradiance was from Equation (8):

$$f = \frac{\cos(\theta_{sen})}{\cos(\theta_{sun})}. \tag{8}$$

The final correction was estimated from Equation (9):

$$E_s = \frac{E_s(\text{obs})}{(1 + d_t(f-1))}. \tag{9}$$

There are limitations to this correction in that it applies to only small angles. Where the angle of tilt is large, the Fresnel reflectance of the 'roughened' sea surface becomes significant when the buoy leans towards the anti-solar direction. For small angles, an error of 2% was assumed, increasing to 4% at lower wavelengths where aerosol and Rayleigh scattering dominated.

The self-shading correction for $L_w(\lambda)$, derived from in-water radiometric measurements, was based on the model of Gordon and Ding (1992) and this correction followed the ocean optics protocols for satellite ocean colour sensor validation (Mueller 2003). The correction required the spectral absorption coefficient $a(\lambda)$, which is approximated to $K_d(\lambda)$, and the quantity h, which is the ratio of diffuse to direct irradiance.

The direct and diffuse irradiances were calculated following Bird and Riordan (1986) and modified to use the extraterrestrial irradiances from Thuillier et al. (2003). The ozone concentration was extracted from the Total Ozone Mapping Spectrometer (available online on website http://ozoneaq.gsfc.nasa.gov/ozone_overhead_all_v8.md); water vapour concentration and AOT were obtained from the MICROTOPS II (version 5.5) sunphotometer (Morys et al. 2001), although for the 2008 and 2009 data these parameters were taken from the MERIS matchup pixel. The total irradiance was used as a check on the $E_s(\lambda)$ derived from the normalization.

Finally, all these measurements were used to estimate the water-leaving reflectance, $\rho_w(\lambda)$, from Equation (10). The radiometric data were determined at the MERIS wavelengths using linear interpolation of the hyperspectral data. This was appropriate since the bandwidth of the Satlantic radiometer is between 10 and 12 nm.

$$\rho_w = \pi \frac{L_w(\lambda)}{E_s(\lambda)}. \tag{10}$$

3.3. *Inter-comparison with other radiometric instruments*

The uncertainties and the accuracy of the *in situ* radiometric data obtained by the Portuguese Satlantic TACCS were assessed during 2010 by inter-comparison with other radiometers used by the MERIS Validation Team (MVT) supported by ESA. In February 2010, there was a field inter-comparison and validation exercise at Sagres between the Portuguese hyperspectral and the Swedish Satlantic TACCS with filters set for MERIS wavelengths. The details of this comparison are presented in Moore, Icely, and Kratzer (2010).

The second inter-comparison, under the title Assessment of *In Situ* Radiometric Capabilities for Coastal Water Remote Sensing Applications (ARC), was conceived within the framework of the MVT. The ARC activities occurred during July 2010 with a phase of field measurements carried out at the AAOT in the north Adriatic Sea over four days characterized by favourable illumination and sea state conditions. The subsequent phase comprised an inter-calibration of the optical sensors deployed at the AAOT. This inter-calibration was achieved at the Joint Research Centre, Ispra Italy, through the absolute radiometric calibration of the optical sensors using identical laboratory standards and methods. These activities quantified differences among fundamental radiometric products derived from the deployment of three in-water and three above-water systems, with the Wire-Stabilized Profiling Environmental Radiometer (WiSPER) and the Portuguese and the Swedish TACCS comprising the in-water systems, and the SeaWiFS Photometer Revision for Incident Surface Measurements (SeaPRISM) and Belgium and Estonian TriOS Optical Systems (TRIOS) comprising the above-water systems. The results from ARC 2010 are presented in Zibordi et al. (2012).

The uncertainties established during the inter-comparisons at Sagres and Venice for the *in situ* radiometric data from the Portuguese TACCS were used to assess the uncertainties for ρ_w at 443, 490, and 560 nm for the three stations off Sagres. Table 2 shows values between 7 and 7.4% for Station A, between 7.1 and 7.2% for Station B, and between 7.6 and 8.1% for Station C.

3.4. Processing satellite data from MERIS

MERIS Level 1b images were processed to Level 2 with the Optical Data processor of ESA, version 8.1 (ODESA MEGS®; see earth.eo.esa.int/odesa/). Full resolution (FR) Level 2 data from MERIS, with a spatial resolution of 290 × 260 m, were obtained with the Basic ERS & ENVISAT (A)ATSR and MERIS Toolbox (BEAM version 4.9; see www.brockmann-consult.de/cms/web/beam/). Based on the coordinates of the stations from each field campaign at Sagres, 3 × 3 pixel matrices were extracted from the MERIS Level 2 products. A matrix was only compared with *in situ* data provided there were five or more valid pixels. Using these procedures, it was possible to evaluate the performance of the different combinations available from the MERIS processor: NoVIC, VIC, ICOL, and VIC + ICOL (see Section 1 for more details). Essentially, the Level 2 procedure started with the NoVIC combination where the images were filtered for contamination such as high glint, ice haze, and high solar zenith. These images could then be configured further by VIC, where a systematic bias to the spectral gains in the radiometric calibration and/or the TOA correction could be corrected by the coefficients shown in Figure 2 (adapted from Table 3 in Lerebourg et al. 2011). MERIS Level 1b images were also processed by ICOL version 2.7.4 with BEAM software version 4.9 and up to Level 2 with the ODESA MEGS® software. Santer (2010) presents the scientific basis for ICOL (see Section 1).

3.5. Statistical methods for the matchup analysis

An analysis of the results from the matchups uses several statistical indicators to quantify the agreement between satellite Level 2 products (y_i) and *in situ* measurements (x_i), including the mean ratio (MR) in Equation (11), the absolute percentage difference (APD) in Equation (12), the average of relative percentage difference (RPD) in

Table 3. Number of matchups (N) with potential for MERIS validation in Sagres (Initial). Number of matchups after processing procedures, without vicarious adjustment (NoVIC); with vicarious adjustment (VIC); with ICOL processing (ICOL); with vicarious adjustment and ICOL processing (VIC+ ICOL) at Station A (SA), Station B (SB), and Station C (SC).

N	SA	SB	SC
Initial	134	131	128
NoVIC	90 (67%)	108 (82%)	115 (90%)
VIC	103 (77%)	97 (74%)	115 (90%)
ICOL	51 (38%)	108 (82%)	113 (88%)
VIC+ ICOL	85 (63%)	113 (86%)	115 (90%)

Equation (13), and also the intercept, slope, and R^2 from linear regressions. In the following, i is the matchup index and N is the number of matchups:

$$\mathrm{MR} = \frac{1}{N}\sum_{i=1}^{N}\frac{y_i}{x_i}, \tag{11}$$

$$\mathrm{APD} = \frac{1}{N}\sum_{i=1}^{N}\left(\frac{|y_i - x_i|}{x_i}\right) 100\ \%, \tag{12}$$

$$\mathrm{RPD} = \frac{1}{N}\sum_{i=1}^{N}\frac{y_i - x_i}{x_i} 100\ \%. \tag{13}$$

4. Results

4.1. Matchup analysis

The number of potential matchups between *in situ* ρ_w and MERIS ρ_w throughout the sampling campaigns is shown in Table 3, with 134, 131, and 128 at Stations A, B, and C, respectively. However, these numbers are reduced during the MEGS processing with different combinations of NoVIC, VIC, ICOL, and VIC + ICOL. The lowest percentage reduction in matchup values occurs uniformly at Station C across the four procedures. On the other hand, the greatest percentage reduction in matchup values occurs at Station A for ICOL followed by VIC + ICOL, with VIC showing the best number of matchups for Station A. In contrast, the greatest percentage reduction in matchup values at Station B is for VIC, with the other three procedures showing similar values.

A comparison of the four combinations used on the matchup data is shown in Figure 4, where scatter plots relate MERIS ρ_w on the y-axis to *in situ* ρ_w on the x-axis for wavelengths 443, 490, and 560 nm; these are considered the most important bandwidths contributing to the MERIS API 1 algorithm. The uncertainty values for ρ_w from Table 2 are represented as horizontal error bars in Figure 4. In general, at oceanic Station C, there are reasonable R^2 values of between 0.74 and 0.86 for the regression analyses of the NoVIC, VIC, ICOL, and VIC + ICOL combinations. However, at the inner Stations A and B there is considerable variation between the R^2 values; most of the low values occur at the coastal Station A for ICOL (R^2 from 0.33 to 0.61), but at Station B there is a marked improvement for ICOL (R^2 from 0.61 to 0.80). At Station A, the best values are for NoVIC (R^2 from 0.44 to 0.69) and VIC + ICOL (R^2 from 0.59 to 0.76), whereas at Station B, the best values are for NoVIC (R^2 from 0.66 to 0.82).

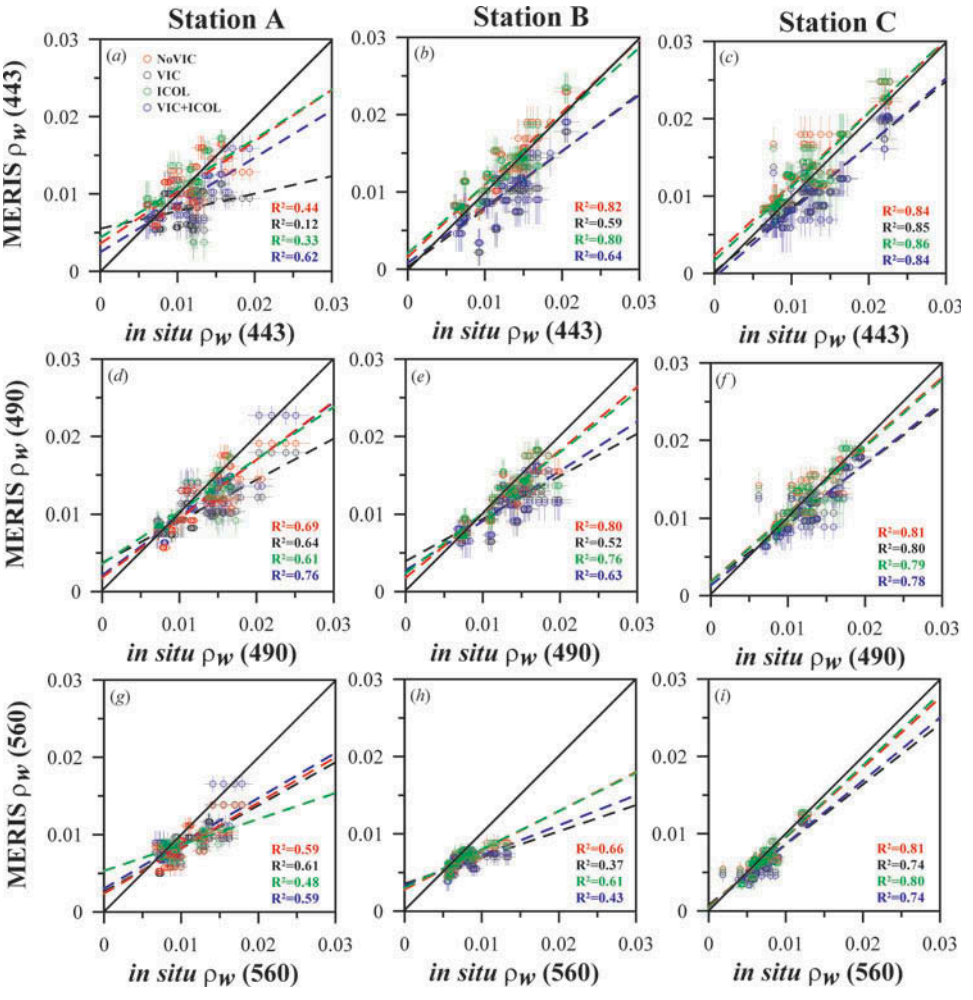

Figure 4. Scatter plots of MERIS water-leaving reflectance (ρ_w) *versus in situ* ρ_w at 443, 490, and 560 nm for Stations A, B, and C. The 1:1 relationship is represented by the solid diagonal line, whereas the linear regression for the data set is represented by the dashed lines. For each matchup point, the vertical bar indicates one standard deviation within the 3 × 3 pixel box used for the matchup and the horizontal bar represents the uncertainty budget for *in situ* ρ_w. Colours represent the different processing combinations with NoVIC (red), VIC (black), ICOL (green), and VIC + ICOL (blue).

The histograms in Figures 5(*a*)–(*i*) show the percentage difference from the mean values of ρ_w at wavelengths 443, 490, and 560 nm for the three stations and for the four different combinations for MERIS processing under evaluation. The lowest percentage differences between the data sets are at 560 nm (Figures 5(*g*)–(*i*)) increasing at 490 nm (Figures 5(*d*)–(*f*)), to the highest at 443 nm (Figures 5(*a*)–(*c*)). The lowest percentage difference between the data sets for the stations is Station C, increasing at Station B to the highest at Station A. In general, the lowest differences for the procedures can be attributed to NoVIC with the exception of Station A for VIC and ICOL at 490 and 560 nm and, finally, at Station C for ICOL at 560 nm.

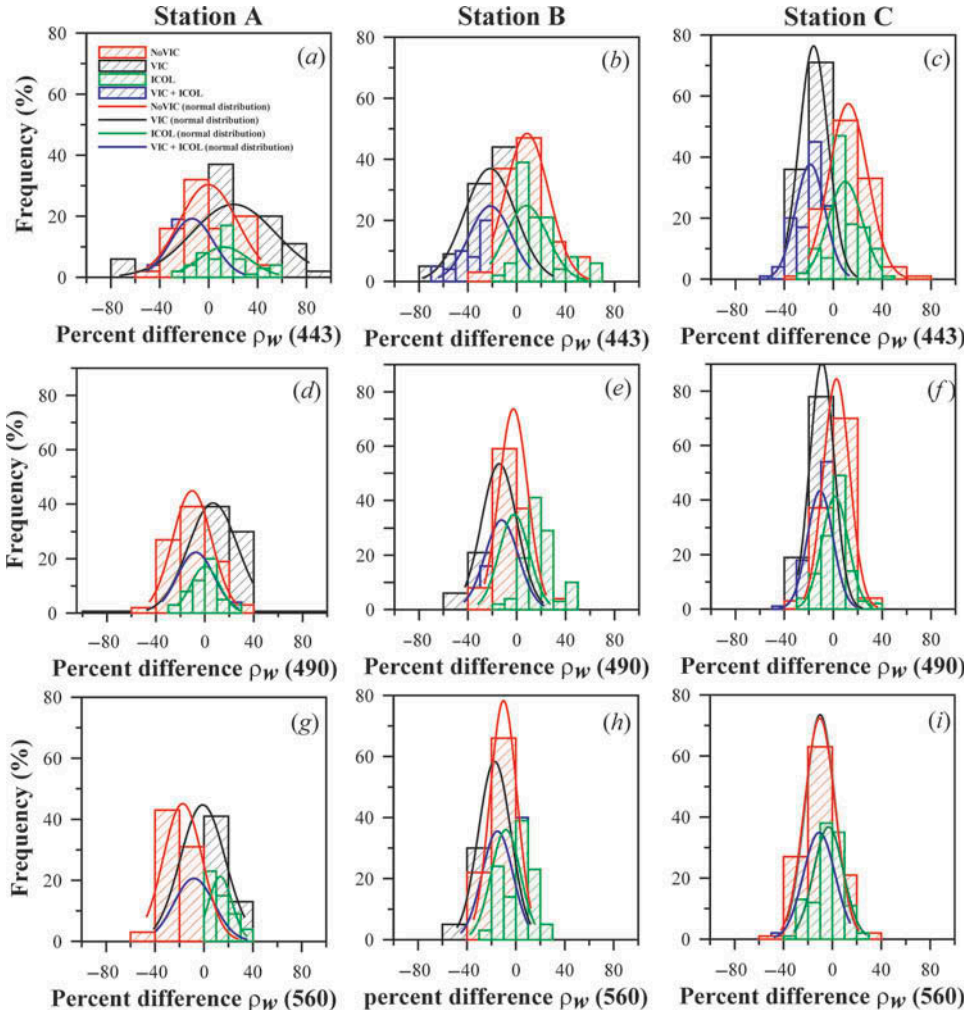

Figure 5. Histograms showing percentage differences for water-leaving reflectance (ρ_w) and curves for normal fit at 443, 490, and 560 nm for Stations A, B, and C. Colours represent the different processing combinations with NoVIC (red), VIC (black), ICOL (green), and VIC + ICOL (blue).

The effect of the four combinations on the quality of the matchup data is analysed in more detail from the statistical analysis for each procedure at wavelengths representing the visible spectrum, including 412, 443, 490, 510, and 665 nm. In addition to the R^2 from the regression analysis, MR, RPD, and APD are considered. The MERIS ρ_w is underestimated relative to the *in situ* ρ_w, where MR <1 and RPD <0, whereas, conversely, the MERIS ρ_w is overestimated where MR >1 and RPD > 0.

The statistical analyses for the procedures NoVIC, VIC, ICOL, and VIC+ ICOL are summarized in Tables 4, 5, 6, and 7, respectively. For NoVIC, MERIS ρ_w is underestimated for 443–665 nm, 490–665 nm, and 560–665 nm at Stations A, B, and C, respectively. For VIC, MERIS ρ_w is underestimated for 560–665 nm at Station A and for all wavelengths at Stations B and C. For ICOL, MERIS ρ_w is underestimated for 510–665 nm, 490–665 nm, and 560–665 nm at Stations A, B, and C, respectively. For

Table 4. Matchup statistics for MERIS water-leaving reflectance (ρ_w) for Stations A, B, and C with NoVIC.

	Station A (N = 90)						Station B (N = 108)						Station C (N = 115)					
λ (nm)	R^2	Intercept	Slope	MR	RPD (%)	APD (%)	R^2	Intercept	Slope	MR	RPD (%)	APD (%)	R^2	Intercept	Slope	MR	RPD (%)	APD (%)
412	0.177	0.007	0.540	1.166	16.6	27.5	0.705	0.003	0.925	1.203	20.3	22.7	0.714	0.005	0.854	1.242	24.2	26.3
443	0.441	0.004	0.662	0.998	−0.2	20.5	0.816	0.002	0.936	1.084	8.4	13.5	0.835	0.002	0.927	1.133	13.3	16.7
490	0.690	0.002	0.757	0.895	−10.5	16.4	0.800	0.002	0.819	0.972	−2.8	10.0	0.806	0.002	0.877	1.037	3.7	9.4
510	0.691	0.002	0.709	0.866	−13.4	17.5	0.721	0.003	0.661	0.950	−5.0	10.0	0.675	0.002	0.811	1.014	1.4	9.0
560	0.586	0.002	0.588	0.826	−17.4	20.6	0.660	0.003	0.506	0.899	−10.1	11.6	0.811	0.000	0.904	0.912	−8.8	14.4
665	0.224	0.000	0.584	0.162	−83.8	84.4	0.358	0.000	0.498	0.458	−54.2	54.2	0.482	0.000	0.823	0.730	−27.0	36.5

Table 5. Matchup statistics for MERIS water-leaving reflectance (ρ_w) for Stations A, B, and C with VIC.

	Station A (N = 103)						Station B (N = 97)						Station C (N = 115)					
λ (nm)	R^2	Intercept	Slope	MR	RPD (%)	APD (%)	R^2	Intercept	Slope	MR	RPD (%)	APD (%)	R^2	Intercept	Slope	MR	RPD (%)	APD (%)
412	0.01	0.008	−0.101	1.359	35.9	47.9	0.422	0.000	0.687	0.699	−30.1	32.5	0.770	0.000	0.755	0.772	−22.8	24.7
443	0.118	0.006	0.226	1.204	20.4	31.9	0.586	0.000	0.746	0.782	−21.8	24.1	0.853	0.000	0.820	0.847	−15.3	17.6
490	0.644	0.004	0.532	1.067	6.7	17.2	0.518	0.004	0.546	0.857	−14.3	16.8	0.795	0.002	0.754	0.916	−8.4	11.8
510	0.667	0.003	0.529	1.041	4.1	16.2	0.362	0.006	0.322	0.838	−16.2	17.3	0.590	0.003	0.574	0.905	−9.5	12.8
560	0.605	0.003	0.557	0.990	−1.0	14.6	0.373	0.004	0.339	0.826	−17.4	18.4	0.742	0.001	0.779	0.912	−8.8	14.4
665	0.094	0.000	0.379	0.951	−4.9	37.6	0.185	0.000	0.484	0.381	−61.9	62.9	0.321	0.000	0.663	0.667	−33.3	41.3

Table 6. Matchup statistics for MERIS water-leaving reflectance (ρ_w) for Stations A, B, and C with ICOL.

	Station A (N = 51)						Station B (N = 108)						Station C (N = 113)					
λ (nm)	R^2	Intercept	Slope	MR	RPD (%)	APD (%)	R^2	Intercept	Slope	MR	RPD (%)	APD (%)	R^2	Intercept	Slope	MR	RPD (%)	APD (%)
412	0.121	0.007	0.503	1.283	28.3	31.8	0.696	0.004	0.851	1.185	18.5	20.9	0.797	0.004	0.912	1.207	20.7	23.1
443	0.336	0.004	0.638	1.125	12.5	18.8	0.796	0.002	0.886	1.079	7.9	13.0	0.857	0.002	0.955	1.106	10.6	14.5
490	0.612	0.004	0.673	1.003	0.3	9.0	0.756	0.002	0.780	0.979	–2.1	10.2	0.793	0.002	0.871	1.025	2.5	9.0
510	0.497	0.005	0.544	0.970	–3.0	10.4	0.660	0.004	0.617	0.963	–3.7	10.0	0.664	0.002	0.806	1.006	0.6	9.0
560	0.476	0.005	0.335	0.917	–8.3	13.4	0.611	0.003	0.495	0.918	–8.2	11.3	0.798	0.000	0.926	0.666	–33.4	11.6
665	0.216	0.001	0.300	0.758	–24.2	29.1	0.372	0.000	0.498	0.645	–35.5	38.4	0.483	0.000	0.855	0.754	–24.6	35.0

Table 7. Matchup statistics for MERIS water-leaving reflectance (ρ_w) for Stations A, B, and C with VIC + ICOL.

	Station A (N = 85)						Station B (N = 113)						Station C (N = 115)					
λ (nm)	R^2	Intercept	Slope	MR	RPD (%)	APD (%)	R^2	Intercept	Slope	MR	RPD (%)	APD (%)	R^2	Intercept	Slope	MR	RPD (%)	APD (%)
412	0.362	0.003	0.448	0.785	–20.8	23.8	0.459	0.001	0.640	0.727	–27.3	30.2	0.785	–0.001	0.813	0.734	–26.6	28.1
443	0.620	0.002	0.611	0.864	–13.0	18.4	0.640	0.001	0.724	0.809	–19.1	23.2	0.844	0.000	0.857	0.819	–18.1	19.9
490	0.757	0.002	0.744	0.926	–6.8	13.6	0.631	0.003	0.638	0.876	–12.4	15.1	0.779	0.001	0.783	0.902	–9.8	12.6
510	0.706	0.002	0.711	0.927	–6.7	13.0	0.523	0.004	0.459	0.861	–13.9	15.4	0.567	0.003	0.604	0.898	–10.2	12.9
560	0.593	0.003	0.585	0.918	–7.6	14.2	0.433	0.003	0.389	0.850	–15.0	15.9	0.738	0.001	0.816	0.907	–9.3	14.7
665	0.134	0.001	0.236	0.821	–17.0	24.0	0.247	0.000	0.544	0.571	–42.9	44.6	0.328	0.000	0.715	0.696	–30.4	38.2

VIC + ICOL, MERIS ρ_w is underestimated for all the wavelengths for all three stations. Wavelengths not included in the above list are those where MERIS ρ_w is overestimated, which are generally in the blue bands (412–490 nm).

The quality of the R^2, MR, RPD, and APD tends to be better at wavelengths 443, 490, and 510 nm and worse at 412 and 560 nm, with the worst wavelength at 665 nm for all four procedures. There is also a trend towards improving statistical results from Station A to Station C.

4.2. *Comparisons of the effects of ICOL processing*

Using all the matchup data it has been possible to trace the effect of ICOL on ρ_w reflectance from the coast to 24 km offshore incorporating all three of the validation stations. Figure 6 displays transects for ρ_w at 490 and 560 nm for the various combinations that are used for the matchup data and shows examples of the four 'classes' of profiles that could be identified along these transects. On 17 November 2008, the first 'class' shows a peak between 3 and 8 km from the shore (Figures 6(*a*), (*b*)); on 27 May 2009, the second 'class' shows no improvement near shore (Figures 6(*c*), (*d*)); on 18 March 2011, the third 'class' shows a marked improvement near shore (Figures 6(*e*), (*f*)); and finally on 24 November 2011, the fourth 'class' shows a dip between 3 and 8 km from the shore (Figures 6((*g*), (*h*)).

MERIS images from the same dates as the transects above are presented in Figure 7, showing the spatial distribution of ρ_w at 560 nm off Sagres for NoVIC, VIC, ICOL, and VIC + ICOL processing. Compared to NoVIC, there is a reduction in the number of invalid reflectances (black areas in the image) for all four dates after ICOL processing, particularly, on 18 March 2011. In contrast, the VIC processing shows little difference with the NoVIC processing on 17 November 2008 and 24 November 2011, whereas it is markedly worse on 27 May 2009 and 18 March 2011. Finally, the combination of VIC + ICOL does show some reduction in the number of invalid reflectances, but not as great as for ICOL on its own.

5. Discussion

5.1. *General*

The Sagres validation campaigns conform to the OPBG criteria, including the following: adherence to the MERIS protocols (Doerffer 2002) for the MERIS sensor; an objective procedure for removing suspect data; a restriction of coincidence time between *in situ* and satellite data records to 0.5 hour for the coastal Station A and up to 1.5 hour for the more offshore Stations B and C. This has resulted in between 272 and 315 matchups over the duration of the sampling campaigns between October 2008 and November 2011, depending on which of the four combinations is used during the MERIS processing. Uncertainties of 8% can be ascribed to these values, based on the various inter-calibration exercises carried out over the duration of the samplings campaigns (Moore, Icely, and Kratzer 2010; Zibordi et al. 2012).

The statistical analysis of the validation data for the NoVIC, VIC, ICOL, and ICOL + VIC procedures shows that the greatest statistical differences occur at the extremes of the visible spectra. This is to be expected as ρ_w at 412 nm is strongly dependent on the accuracy of the atmospheric correction procedure (Antoine, d'Ortenzio, et al. 2008), and ρ_w at 665 nm has low values in Case 1 waters. Table 8 compares the statistical analysis for

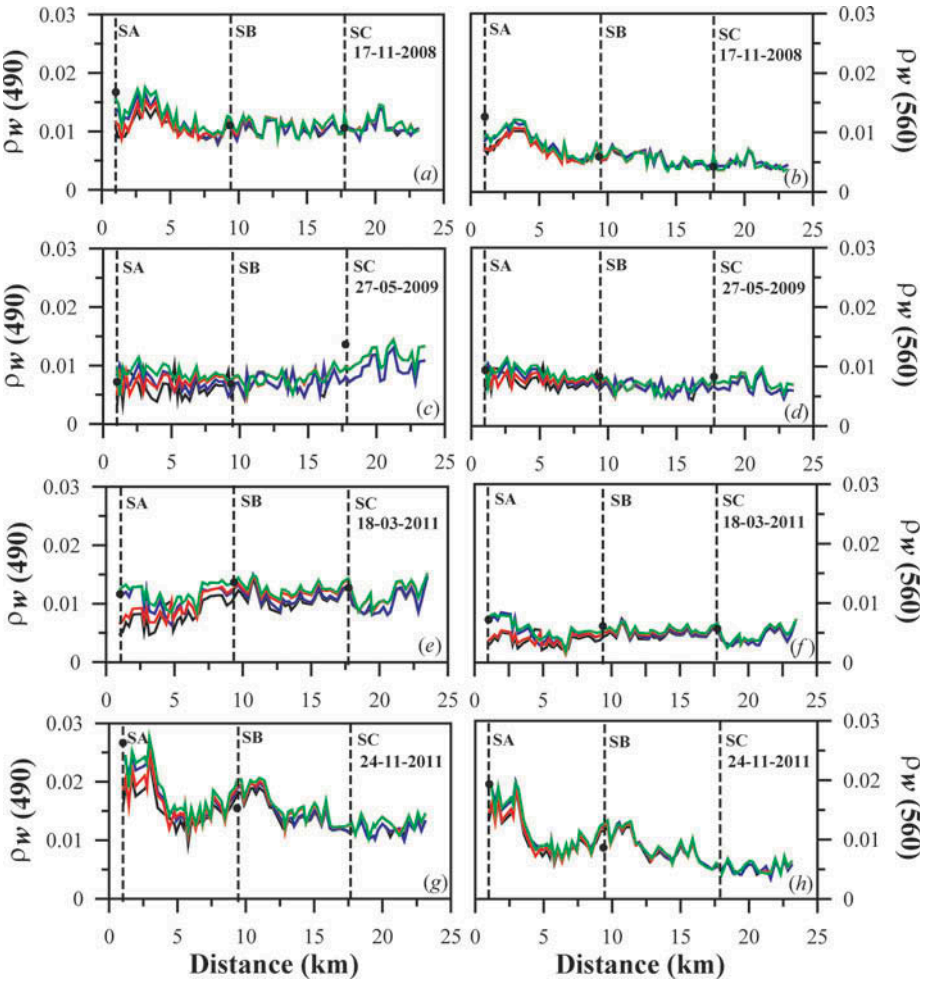

Figure 6. Transects of water-leaving reflectance (ρ_w) at 490 and 560 nm for 17 November 2008, 27 May 2009, 18 March 2011, and 24 November 2011 extending perpendicular from the coast up to approximately 24 km offshore. Each trace has undergone different processing combinations with NoVIC in red, VIC in black, ICOL in green, and VIC + ICOL in blue. The dashed vertical lines indicate the approximate locations of Stations A, B, and C from the coast with the value for *in situ* ρ_w shown as full black circles.

NoVIC calibration between the three Sagres sites with AAOT (Zibordi, Mélin, and Berthon 2006), BOUSSOLE (Antoine, d'Ortenzio, 2008), and the Bohai Sea (Cui et al. 2010) for 443, 490, and 560 nm. In general at AAOT and BOUSSOLE, MERIS ρ_w is overestimated relative to the *in situ* data, whereas at Sagres and Bohai they tend to be underestimated. The R^2 is best for AAOT, but is also good at Stations B and C at Sagres.

The statistics for the bio-optical properties at Sagres in Table 1 and the ternary diagrams in Figure 3 demonstrate that the bio-optical properties between the coastal Station A and the more oceanic Station C are consistently similar and are essentially Case 1; the elevated values for YS may be linked to the upwelling phenomena of the area, as a similar variance is observed in the NOMAD database, which contains data from a number of upwelling regions. It is evident that the Sagres Station C has more in common

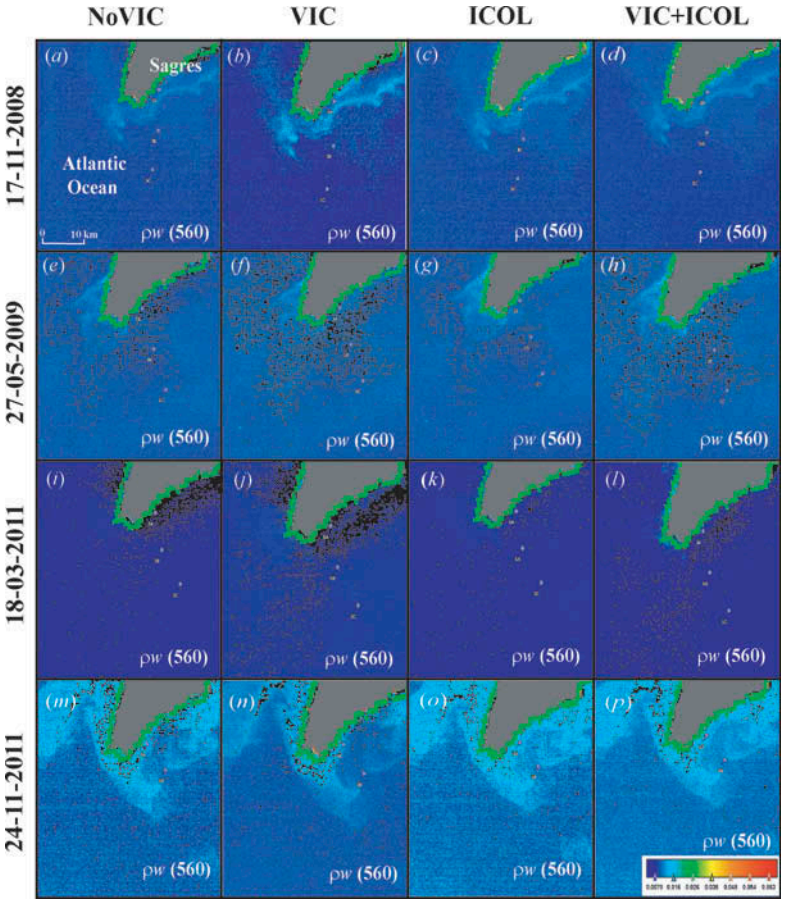

Figure 7. Water-leaving reflectance (ρ_w) at 560 nm from MERIS full-resolution satellite images from 17 November 2008, 27 May 2009, 18 March 2011, and 24 November 2011 at similar coordinates for the stations shown in Figure 1. Each date shows images with different processing combinations NoVIC, VIC, ICOL, and VIC + ICOL.

with the deep, offshore site for BOUSSOLE, where the conditions remain predominately Case 1 (Antoine et al. 2008a), than with more turbid coastal conditions of the Bohai Sea (Cui et al. 2010) or, even for AAOT (Zibordi, Mélin, and Berthon 2006; Zibordi et al. 2013), where conditions are often Case 2. Antoine, d'Ortenzio, (2008) suggest that MERIS products in terms of the atmospheric correction do not meet the required 5% level of accuracy at 443 and 490 nm. However, Table 9 compares the statistics between BOUSSOLE and the offshore Station C for Sagres and show that the matchups between MERIS ρ_w and *in situ* ρ_w are substantially better at Sagres.

5.2. *Vicarious calibration*

Both studies Zibordi, Mélin, and Berthon (2006) and Antoine, d'Ortenzio, et al. (2008) recommended the use of vicarious calibration for improving the calibration of the MERIS sensor. However, the early versions of MEGS processing did not have the capacity for VIC calibration/adjustment, which is why Tables 8 and 9 only present data for NoVIC.

Table 8. Comparison of published statistical data for MERIS matchups with those at Sagres for wavelengths 443, 490, and 560 nm, where N = number of matchups, R^2 = coefficient of determination, MR = mean ratio, RPD = relative percentage difference, and APD = absolute percentage difference.

	AAOT (Zibordi, Mélin, and Berthon 2006)			BOUSSOLE (Antoine, Guevel, et al. 2008)			Bohai Sea (Cui et al. 2010)			Sagres Station A			Sagres Station B			Sagres Station C		
	443	490	560	443	490	560	443	490	560	443	490	560	443	490	560	443	490	560
N	41	41	41	61	64	63	13	13	13	103	103	103	97	97	97	115	115	115
R^2	0.79	0.92	0.95	0.38	0.44	0.34	0.55	0.41	-0.01	0.12	0.64	0.61	0.59	0.52	0.37	0.85	0.80	0.74
MR	–	–	–	1.32	1.16	1.21	–	–	–	1.20	1.07	0.99	0.78	0.86	0.83	0.85	0.92	0.91
RPD (%)	42	21	15	31.6	15.8	21.3	–10	1	5	20.4	6.7	–1.0	–21.8	–14.3	–17.4	–15.3	–8.4	–8.8
APD (%)	43	22	18	35.8	18.6	25.3	18	15	16	31.9	17.2	14.6	24.1	16.8	18.4	17.6	11.8	14.4

Table 9. Matchup statistics for MERIS water-leaving reflectance (ρ_w) comparing BOUSSOLE (Antoine, Guevel, et al. 2008) with Station C at Sagres. The sample numbers (N) for BOUSSOLE are 20, 61, 64, 63, 64, and 64 for the wavelengths 412, 443, 490, 510, 560, and 665 nm, respectively. At Sagres, $N = 115$ for all the wavelengths listed in the Table.

	BOUSSOLE					Station C				
λ (nm)	R^2	Intercept	Slope	RPD (%)	APD (%)	R^2	Intercept	Slope	RPD (%)	APD (%)
412	0.43	0.009	0.93	60.2	62.7	0.71	0.005	0.854	24.2	26.3
443	0.38	0.008	0.70	31.6	35.8	0.83	0.002	0.927	13.3	16.7
490	0.44	0.006	0.69	15.8	18.6	0.81	0.002	0.877	3.7	9.4
510	0.24	0.007	0.52	21.5	23.5	0.67	0.002	0.811	1.4	9
560	0.34	0.003	0.64	21.3	25.3	0.81	0.000	0.904	−8.8	14.4
665	0.16	0.001	0.89	59	69.1	0.48	0.000	0.823	−27	36.5

Despite the advocacy of Zibordi, Mélin, and Berthon (2006) and Antoine, d'Ortenzio, et al. (2008) for VIC, the study at Sagres shows mixed statistical results when comparing NoVIC and VIC, with generally worse R^2 for VIC; the MR, RPD, and APD are also generally worse, except at Station A. Indeed, a comparison of the slope for NoVIC and VIC at Sagres (Tables 4 and 5, respectively) shows that the slope for the regression analysis is better for NoVIC at all three stations and at all the selected wavelengths compared to VIC.

A more recent study by Zibordi et al. (2013), where the results from MEGS-7 are compared with those from MEGS 8.1, found the statistical results for VIC calibration relating MERIS water leaving radiance (L_{wn}) with *in situ* L_{wn} from AAOT site to be strikingly similar to those relating MERIS ρ_w to *in situ* ρ_w at Station C in Sagres, despite using very different measurement procedures. Table 10 shows R^2, RPD, and APD for these comparisons at both AAOT and Station C at Sagres, and includes a further study by Kajiyama, D'Alimonte, and Zibordi (2014) for AAOT. As an example, all three studies showed a negative bias for RPD at all the wavelengths, after using the VIC combination during MEGS 8.1, indicating an underestimation for MERIS L_{wn} or ρ_w, particularly at the more extreme wavelengths. Nonetheless, the Sagres data do show some differences compared to the AAOT data (Zibordi et al. 2013; Kajiyama, D'Alimonte, and Zibordi 2014), with better statistics at 412 nm and worse statistics at 665 nm for Sagres relative to those for the same wavelengths at AAOT. The probable explanation for these differences is that the conditions are more turbid at AAOT, increasing the scatter in the *in situ* L_{wn} values in the red, compared with those at Sagres, which are close to the limits of detection. At extreme blue wavelengths the *in situ* L_{wn} is similar at both sites, but the atmospheric turbidity is on average greater at AAOT, resulting in atmospheric correction errors.

One of the potential advantages of vicarious adjustment is to ensure compatibility between measurements from different satellites. However, the slopes for the MERIS matchup statistics at Station C for both NoVIC (Table 4) and VIC (Table 5) are comparable with those from the MERIS third reprocessing validation report (e.g. Figure 5 in MQWG 2012), where the MERIS radiometric data is generally lower relative to SeaWIFS and MODIS products.

5.3. *Improved contrast between ocean and land*

At Sagres, particularly at the inner Station close to the coast, it is clear that coastal adjacency is modifying the atmospheric correction, probably due to reflectances from the

Table 10. Comparison of MERIS matchups from AAOT site (*Zibordi et al. 2013; †Kajiyama, D'Alimonte, and Zibordi 2014) with Sagres ocean Station C with MERIS water-leaving reflectance (ρ_w) after NoVIC in bold italics and after VIC in normal text for wavelengths 413, 443, 490, 560, and 665 nm, where N = number of matchups, R^2 = coefficient of determination, RPD = relative percentage difference, and APD = absolute percentage difference.

	AAOT (N = 160)*			AAOT (N = 86)*			AAOT (N = 100)†			Sagres (N = 115)			Sagres (N = 115)		
λ (nm)	R^2	RPD (%)	APD (%)	R^2	RPD (%)	APD (%)	R^2	RPD (%)	APD (%)	R^2	RPD (%)	APD (%)	R^2	RPD (%)	APD (%)
412	***0.19***	***55***	***69***	0.43	–40	48	0.39	–43	44	***0.71***	***24.2***	***26.3***	0.77	–23	25
443	***0.46***	***17***	***36***	0.71	–23	29	0.67	–26	26	***0.83***	***13.3***	***16.7***	0.85	–15	18
490	***0.80***	***11***	***17***	0.88	–8	14	0.81	–12	14	***0.81***	***3.7***	***9.4***	0.80	–8	12
560	***0.90***	***7***	***15***	0.91	–2	12	0.88	–8	12	***0.81***	***–8.8***	***14.4***	0.74	–9	14
665	***0.82***	***–4***	***44***	0.80	–16	33	0.77	28	36	***0.48***	***–27***	***36.5***	0.32	–23	41

vegetation cover over the land fluctuating with the seasonal changes during the year. Thus satellite-derived marine reflectance near the coast is underestimated due to errors in the atmospheric correction caused by Rayleigh and aerosol scattering from the nearby land surface (Santer 2010). ICOL has been developed to improve these coastal adjacency errors for MERIS products (Santer and Schmechtig, 2000). On the basis of the striking uniformity between the characteristics of the stations at Sagres, these coastal waters should be useful for testing ICOL. Furthermore, the atmospheric conditions can be estimated from the local AERONET station, and the vegetation cover over the land fluctuates only relatively slowly with the seasons. Nonetheless, the scatter plots in Figure 4 and the poor statistical data for Station A (Tables 6, 7) suggest that the outcome of ICOL processing is inconsistent at Sagres, particularly close to the coast. However, Figure 7 does show consistent improvement in the MERIS images for ρ_w at 560 nm after ICOL processing. Although most of the effects of ICOL occur within the initial 8 km offshore, there are certain conditions when the adjacency correction is affecting the offshore site at 18 km. This can be inferred from the shift in slope towards the 1:1 from NoVIC (Table 4) to ICOL (Table 6) after changes in combination during MERIS processing. It is evident that ICOL needs to be studied in more detail at Sagres, but there are further considerations that might explain at least some of the observed differences.

(1) For the current research, combining ICOL with MEGS 8.1 has to be done offline. As MEGS 8.1 does not correct for adjacency, ICOL has been used to provide TOA reflectance at distinct wavelengths corrected for adjacency effects. However, the Rayleigh correction assumes that there is a specular rather than a Lambertian surface adjacent to the viewed pixel and, therefore, there is an error for the Fresnel reflectance assumed by MEGS 8.1. This could explain those transects where there are large peaks or dips in ρ_w over the range 3–8 km from the shore, consistent with the Rayleigh scale height (e.g. Figures 6(*a*), (*b*), (*g*), and (*h*)).
(2) It could be argued that bottom effects may be affecting the results close to the coast, but this is not the situation at Sagres where depths are substantially greater than 5 optical depths, even at the near-shore Station A (+40 m). It is possible that some differences are related to the changes in the bio-optical properties of the water linked to upwelling events.
(3) Land reflectances may influence the atmospheric correction (AC) due to changes in vegetation cover during the seasons. As ICOL only performs a simple AC over land, the effect of vegetation is to produce changes in the spectral regions 680–740 nm (NIR), and there does seem to be more anomalous results from ICOL during spring and autumn as opposed to summer.

Kratzer and Vinterhav (2010) tested the ICOL processor in combination with three other processors for MERIS images of the Himmerfjärden Bay and the surrounding areas of the northwestern Baltic Sea; the satellite images corrected for adjacency present a significantly better fit with the *in situ* data. However, ICOL has also been tested at Lake Woods (an inland water between USA and Canada) and appears not to improve retrieval of water constituents (Binding et al. 2011).

Although the processing procedures for validation at Sagres have shown equivocal results, it is evident that the data from the stations at Sagres could continue to prove useful for improving the processing procedures for MERIS products, and that this site would be useful for any validation exercises for future ocean colour sensors such as the Ocean and Land Colour Instrument (OLCI) on Sentinel 3.

6. Conclusions

- Approximately 130 matchups between MERIS water-leaving reflectances (ρ_w) and *in situ* measurements have been obtained between 2008 and 2011 for each of three stations at Sagres (A, at 2 km; B, at 10 km; and C, at 18 km).
- These numbers are reduced during the MERIS third reprocessing procedures dependent on the combinations of NoVIC, VIC, ICOL, and with ICOL + VIC: with approximately 20–60% for the inshore Station A; 20% for Station B; and 10% for the offshore Station C.
- The statistical comparison of the matchups between MERIS ρ_w and the *in situ* ρ_w shows a better coefficient of determination, and less uncertainty and bias, at the centre of the visible spectra (490–560 nm) than at the extremes (412 and 665 nm).
- The oceanic Station C at Sagres is of particular interest because it has characteristics in common with both BOUSSOLE and AAOT validation sites. However, vicarious adjustment results in poorer statistics, with the regression slope being closer to unity at all wavelengths without vicarious adjustment. With the exception of the wavelengths 412 and 443 nm for R^2, the intercepts MR, RPD, and APD are better without vicarious adjustment applied. The differences for MR and APD indicate that the vicarious adjustment results in a marginal improvement in these two bands, whereas the RPD indicates that the vicarious is an over-adjustment.
- Overall, Station C, Sagres site, has achieved better matchup statistics for the MERIS sensor than BOUSSOLE (Table 9). The statistics for both NoVIC and VIC are similar to those for AAOT (Table 10). Differences can be attributed to the more turbid conditions at AAOT and low values for the red at Sagres.
- The ICOL processing shows mixed results with improvements to matchups occurring only for some campaigns.
- The uniformity between the bio-optical characteristics of the stations at Sagres indicate that validation data from Sagres is particularly useful for understanding the effects of coastal adjacency on satellite ocean colour products.

Acknowledgements

We would like to thank ESA and ACRI-ST for developing ODESA MEGS® (http://earth.eo.esa.int/odesa); Brockmann Consult for access to the MERIS Level 2 full-resolution satellite images; and to Ricardo and Sara Magalhães for their boat support. We also thank Dr Samantha Lavender and two anonymous referees for improvements to the text.

Funding

This work was funded by the European Space Agency for the 'Technical Assistance for the Validation of MERIS Marine Products at Portuguese oceanic and coastal sites' [21464/08/I-OL]; PhD grants from Fundação para a Ciência e a Tecnologia [SFRH/BD/78354/2011], [SFRH/BD/78356/2011]; supported by the DEVOTES project (http://www.devotes-project.eu/) EC 7th Framework Programme [308392]; and AQUA_USERS project EC 7th Framework Programme [607325].

Supplemental data and underlying research materials

The underlying research materials for this article can be accessed at http://hermes.acri.fr/mermaid/home/home.php – MEris MAtchup In-situ Database (MERMAID).

References

Ahn, Y. H., and P. Shanmugam. 2006. "Detecting the Red Tide Algal Blooms from Satellite Ocean Color Observations in Optically Complex Northeast-Asia Coastal Waters." *Remote Sensing of Environment* 103: 419–437. doi:10.1016/j.rse.2006.04.007.

Antoine, D., F. d'Ortenzio, S. B. Hooker, G. Bécu, B. Gentili, D. Tailliez, and A. J. Scott. 2008. "Assessment of Uncertainty in the Ocean Reflectance Determined by Three Satellite Ocean Color Sensors (MERIS, SeaWiFS and MODIS-A) at an Offshore Site in the Mediterranean Sea (BOUSSOLE Project)." *Journal of Geophysical Research* 113: C07013. doi:10.1029/2007JC004472.

Antoine, D., P. Guevel, J.-F. Desté, G. Bécu, F. Louis, A. J. Scott, and P. Bardey. 2008. "The 'BOUSSOLE' Buoy – A New Transparent-To-Swell Taut Mooring Dedicated to Marine Optics: Design, Tests and Performance at Sea." *Journal of Atmospheric and Oceanic Technology* 25: 968–989. doi:10.1175/2007JTECHO563.1.

Bailey, S. W., and P. J. Werdell. 2006. "A Multi-Sensor Approach for the On-Orbit Validation of Ocean Color Satellite Data Products." *Remote Sensing of Environment* 102: 12–23. doi:10.1016/j.rse.2006.01.015.

Banks, A. C., P. Prunet, J. Chimot, P. Pina, J. Donnadille, E. Jeansou, M. Lux, G. Petihakis, G. Korres, G. Triantafyllou, C. Fontana, C. Estournel, C. Ulses, and L. Fernandez. 2012. "A Satellite Ocean Color Observation Operator System for Eutrophication Assessment in Coastal Waters." *Journal of Marine Systems* 94: S2–S15. doi:10.1016/j.jmarsys.2011.11.001.

Barker, K. 2011. "MERIS Optical Measurements Protocols. Part A: In Situ Water Reflectance Measurements." Revision 1.0, Document No.CO-SCI-ARG-TN-0008.

Behrenfeld, M. J., R. T. O'Malley, D. A. Siegel, C. R. McClain, J. L. Sarmiento, G. C. Feldman, A. J. Milligan, P. G. Falkowski, R. M. Letelier, and E. S. Boss. 2006. "Climate-Driven Trends in Contemporary Ocean Productivity." *Nature* 444: 752–755. doi:10.1038/nature05317.

Binding, C. E., T. A. Greenberg, J. H. Jerome, R. P. Bukata, and G. Letourneau. 2011. "An Assessment of MERIS Algal Products during an Intense Bloom in Lake of the Woods." *Journal of Plankton Research* 33: 793–806. doi:10.1093/plankt/fbq133.

Bird, R. E., and C. J. Riordan. 1986. "Simple Simple Solar Spectral Model for Direct and Diffuse Irradiance on Horizontal and Tilted Planes at the Earth's Surface for Cloudless Atmospheres." *Journal of Climate and Applied Meteorology* 25 (1): 87–97. doi:10.1175/1520-0450(1986)025<0087:SSSMFD>2.0.CO;2.

Broenkow, W. W., D. K. Clark, and M. A. Yarbrough. 1996. *SeaWiFS Optical Buoy for the Hawaii Times Series Experiment.* Final Report NASA Contract RFPR-98012/272. Moss Landing, CA: Moss Landing Marine Laboratories Technical Publication 96-5.

Carvalho, G. A., P. J. Minnett, V. F. Banzon, W. Baringer, and C. A. Heil. 2011. "Long-Term Evaluation of Three Satellite Ocean Color Algorithms for Identifying Harmful Algal Blooms (*Karenia brevis*) along the West Coast of Florida: A Matchup Assessment." *Remote Sensing of Environment* 115: 1–18. doi:10.1016/j.rse.2010.07.007.

Cristina, S., P. Goela, J. Icely, A. Newton, and B. Fragoso. 2009. "Assessment of the Optical Properties of the Ocean and Coastal Waters Using MERIS Satellite Products in Sagres Off the South West Coast of Portugal." *Journal of Coastal Research* 56: 1479–1483.

Cristina, S., J. Icely, P. Goela, and A. Newton. 2010. "Validation of the MERIS Satellite Products in Oceanic Waters Off Cape Sagres on the South-West Coast of Portugal." Paper presented at the Proceedings of the ESA Living Planet Symposium, SP-686, no. 107 European Space Agency, Bergen, June 28–July 2.

Cui, T., J. Zhang, S. Groom, L. Sun, T. Smyth, and S. Sathyendranath. 2010. "Validation of MERIS Ocean-Color Products in the Bohai Sea: A Case Study for Turbid Coastal Waters." *Remote Sensing of Environment* 114: 2326–2336. doi:10.1016/j.rse.2010.05.009.

Doerffer, R. 2002. "Protocols for the Validation of MERIS Water Products." European Space Agency Document No. PO-TN-MEL-GS-0043.

Dowell, M., and T. Platt, eds. 2009. *Partition of the Ocean into Ecological Provinces: Role of Ocean-Colour Radiometry.* Reports of the International Ocean-Colour Coordinating Group, No. 9. Dartmouth: Published by the International Ocean-Colour Coordinating Group.

Eleveld, M. A., R. Pasterkamp, H. J. van der Woerd, and J. D. Pietrzak. 2008. "Remotely Sensed Seasonality in the Spatial Distribution of Sea-Surface Suspended Particulate Matter in the Southern North Sea." *Estuarine, Coastal and Shelf Science* 80: 103–113. doi:10.1016/j.ecss.2008.07.015.

Field, C. B., M. J. Behrenfeld, J. T. Randerson, and P. G. Falkowski. 1998. "Primary Production of the Biosphere: Integrating Terrestrial and Oceanic Components." *Science* 281: 237–240. doi:10.1126/science.281.5374.237.

Franz, B. A., S. W. Bailey, P. J. Werdell, and C. R. McClain. 2007. "Sensor-Independent Approach to the Vicarious Calibration of Satellite Ocean Color Radiometry." *Applied Pptics* 46: 5068–5082. doi:10.1364/AO.46.005068.

Goela, P. C., J. Icely, S. Cristina, A. Newton, G. Moore, and C. Cordeiro. 2013. "Specific Absorption Coefficient of Phytoplankton Off the Southwest Coast of the Iberian Peninsula: A Contribution to Algorithm Development for Ocean Colour Remote Sensing." *Continental Shelf Research* 52: 119–132. doi:10.1016/j.csr.2012.11.009.

Gordon, H., and K. Ding. 1992. "Self-Shading of In-Water Optical Instruments." *Limnology and Oceanography* 37 (3): 491–500. doi:10.4319/lo.1992.37.3.0491.

Gordon, H. R., and A. Morel. 1983. "Remote Assessment of Ocean Color for Interpretation of Satellite Visible Imagery." In *A Review, Lecture Notes on Coastal and Estuarine Studies*, edited by R. T. Barber, N. K. Mooers, M. J. Bowman, and B. Zeitzschel. New York: Springer-Verlag.

Hooker, S. B., C. R. McClain, J. K. Firestone, T. L. Westphal, E.-N. Yeh, and Y. Ge. 1994. *The SeaWiFS Bio-Optical Archive and Storage System (SeaBASS): Part 1. NASA Technical Memorandum Vol. 104566*. Greenbelt, MD: NASA Goddard Space Flight Center.

Kajiyama, T., D. D'Alimonte, and G. Zibordi. 2014. "Match-Up Analysis of MERIS Radiometric Data in the Northern Adriatic Sea." *IEEE Geoscience and Remote Sensing Letters* 11 (1): 19–23. doi:10.1109/LGRS.2013.2244844.

Kratzer, S., C. Brockmann, and G. Moore. 2008. "Using MERIS Full Resolution Data to Monitor Coastal Waters – A Case Study from Himmerfjärden, a Fjord-Like Bay in the Northwestern Baltic Sea." *Remote Sensing of Environment* 112: 2284–2300. doi:10.1016/j.rse.2007.10.006.

Kratzer, S., and C. Vinterhav. 2010. "Improvement of MERIS level 2 Products in Baltic Sea Coastal Areas by Applying the Improved Contrast between Ocean and Land Processor (ICOL) – Data Analysis and Validation." *Oceanologia* 52 (2): 211–236. doi:10.5697/oc.52-2.211.

Kwiatkowska, E. J., B. A. Franz, G. Meister, C. R. McClain, and X. Xiong. 2008. "Cross Calibration of Ocean-Color Bands from Moderate Resolution Imaging Spectroradiometer on Terra Platform." *Applied Optics* 47: 6796–6810. doi:10.1364/AO.47.006796.

Lerebourg, C., C. Mazeran, J. P. Huot, and D. Antoine. 2011. "MERIS ATBD 2.24. Vicarious Adjustment of the MERIS Ocean Colour Radiometry." ACRI-ST. Ref.:MERIS ATBD 2.24 Issue:1.0.

Longhurst, A. 1998. *Ecological Geography of the Sea*. San Diego, CA: Academic Press.

Longhurst, A. 2006. *Ecological Geography of the Sea*. 2nd ed. San Diego, CA: Academic Press Elsevier.

Loureiro, S., A. Newton, and J. D. Icely. 2005. "Microplankton Composition, Production and Upwelling Dynamics in Sagres (SW Portugal) during the Summer of 2001." *Scientia Marina* 69 (3): 323–341.

Loureiro, S., A. Reñé, E. Garcés, J. Camp, and D. Vaqué. 2011. "Harmful Algal Blooms (HABs), Dissolved Organic Matter (DOM), and Planktonic Microbial Community Dynamics at a Near-Shore and a Harbour Station Influenced by Upwelling (SW Iberian Peninsula)." *Journal of Sea Research* 65 (4): 401–413. doi:10.1016/j.seares.2011.03.004

McClain, C. R., J. R. Christian, S. R. Signorini, M. R. Lewis, I. Asanuma, D. Turk, and C. Dupouy-Douchement. 2002. "Satellite Ocean-Color Observations of the Tropical Pacific Ocean." *Deep Sea Research Part II: Topical Studies in Oceanography* 49: 2533–2560. doi:10.1016/S0967-0645(02)00047-4

McClain, C. R., W. E. Esaias, W. Barnes, B. Guenther, D. Endres, S. Hooker, G. Mitchell, and R. Barnes. 1992. "SeaWiFS Calibration and Validation Plan." In *NASA Technical Memorandum 104566*, Vol. 3, edited by S. B. Hooker and E. R. Firestone. Greenbelt, MD: NASA Goddard Space Flight Center.

McCulloch, M. E., K. L. Barker, and G. Zibordi. 2010. "Vicarious Adjustment of MERIS Reflectances Using an Inverse Technique." Paper presented at the Proceedings of the ESA Living Planet Symposium, SP-686, Bergen, June 28–July 2.

Mobley, C. D. 1995. *Hydrolight 3.0 Users Guide.* SRIRI Project 5632. Menlo Park, CA: SRI International.

Moore, G. F., J. D. Icely, and S. Kratzer. 2010. "Field Inter-Comparison and Validation of In-Water Radioamter and Sunphotometers for MERIS Validation." Paper presented at the Proceedings of the ESA Living Planet Symposium, SP-686, Bergen, June 28–July 2.

Morel, A., ed. 1998. *Minimum Requirements for an Operational Ocean-Colour Sensor for the Open Ocean.* Reports of the International Ocean-Colour Coordinating Group, No. 1. IOCCG. Dartmouth: Published by the International Ocean-Colour Coordinating Group.

Morel, A., and D. Antoine. 1994. "Heating Rate within the Upper Ocean in Relation to its Bio-Optical State." *Journal of Physical Oceanography* 24: 1652–1665. doi:10.1175/1520-0485(1994)024<1652:HRWTUO>2.0.CO;2.

Morel, A., and S. Maritorena. 2001. "Bio-Optical Properties of Oceanic Waters: A Reappraisal." *Journal of Geophysical Research* 106: 7163–7180. doi:10.1029/2000JC000319.

Morys, M., F. M. Mims III, S. Hagerup, S. E. Anderson, A. Baker, J. Kia, and T. Walkup. 2001. "Design, Calibration and Performance of MICROTOPS II Handheld Ozone Monitor and Sun Photometer." *Journal of Geophysical Research Atmosphere* 106 (D13): 14573–14582. doi:10.1029/2001JD900103.

MQWG. 2011. "MERIS 3rd Data Reprocessing – Software and ADF Updated." Accessed July 15, 2013. http://earth.eo.esa.int/pcs/envisat/meris/documentation/meris_3rd_reproc/MERIS_3rd_Reprocessing_Changes.pdf

MQWG. 2012. "MERIS 3rd Data Reprocessing: Validation Report." Accessed July 15, 2013. http://earth.eo.esa.int/pcs/envisat/meris/documentation/meris_3rd_reproc/A879-NT-017-ACR_v1.0.pdf

Mueller, J. L. 2003. "In-Water Radiometric Profile Measurements and Data Analysis Protocols." In *Ocean Optics Protocols for Satellite Ocean Color Sensor Validation*, NASA Technical Memorandum – 2003-21621, Rev. 4, Vol. III., edited by J. L. Mueller, G. S. Fargion, and C. R. McClain, 7–19. Greenbelt, MD: NASA.

Newton, A., and J. Icely. 2008. "Land Ocean Interactions in the Coastal Zone, LOICZ: Lessons from Banda Aceh, Atlantis, and Canute." *Estuarine, Coastal and Shelf Science* 77: 181–184. doi:10.1016/j.ecss.2007.09.016.

Petersen, W., H. Wehde, H. Krasemann, F. Colijn, and F. Schroeder. 2008. "FerryBox and MERIS – Assessment of Coastal and Shelf Sea Ecosystems by Combining In-Situ and Remotely Sensed Data." *Estuarine, Coastal and Shelf Science* 77: 296–307. doi:10.1016/j.ecss.2007.09.023

Platt, T., and S. Sathyendranath. 2008. "Ecological Indicators for the Pelagic Zone of the Ocean from Remote Sensing." *Remote Sensing of Environment* 112: 3426–3436. doi:10.1016/j.rse.2007.10.016.

Platt, T., N. Hoepffner, V. Stuart, and C. Brown, eds. 2008. *Why Ocean Colour? The Societal Benefits of Ocean-Colour Technology.* Reports of the International Ocean-Colour Coordinating Group, No. 7, IOCCG. Dartmouth: Published by the International Ocean-Colour Coordinating Group.

Prieur, L., and S. Sathyendranath. 1981. "An Optical Classification of Coastal and Oceanic Waters Based on the Specific Spectral Absorption Curves of Phytoplankton Pigments, Dissolved Organic Matter, and Other Particulate Materials." *Limnology and Oceanography* 26: 671–689. doi:10.4319/lo.1981.26.4.0671.

Rast, M., J. L. Bezy, and S. Bruzzi. 1999. "The ESA Medium Resolution Imaging Spectrometer MERIS- A Review of the Instrument and its Mission." *International Journal of Remote Sensing* 20: 1681–1702. doi:10.1080/014311699212416.

Relvas, P., and E. D. Barton. 2005. "A Separated Jet and Coastal Counterflow during Upwelling Relaxation Off Cape São Vicente (Iberian Peninsula)." *Continental Shelf Research* 25: 29–49. doi:10.1016/j.csr.2004.09.006.

Relvas, P., E. D. Barton, J. Dubert, P. B. Oliveira, Á. Peliz, J. C. B. da Silva, A. Santos, and P. Santos. 2007. "Physical Oceanography of the Western Iberia Ecosystem: Latest Views and Challenges." *Progress in Oceanography* 74: 149–173. doi:10.1016/j.pocean.2007.04.021.

Ruddick, K., G. Lacroix, C. Lancelot, B. Nechad, Y. Park, S. Peters, and B. Van Mol. 2008. "Optical Remote Sensing of North Sea." In *Remote Sensing of the European Seas*, edited by V. Barale and M. Gade, 79–90. Ispra: Springer.

Santer, R. 2010. "ICOL + ATBD." Brockman Consult and University of Littoral, France, Version 1.0, (D4).

Santer, R., and C. Schmechtig. 2000. "Adjacency Effects on Water Surfaces: Primary Scattering Approximation and Sensitivity Study." *Applied Optics* 39: 361–375. doi:10.1364/AO.39.000361.

Santer, R., and F. Zagolski. 2009. "ICOL Improve Contrast between Ocean and Land." ATBD–MERIS level-1C. Revision 1, Report D6 (1), Univ. Littoral, France.

Santos, A. M. P. 2000. "Fisheries Oceanography Using Satellite and Airborne Remote Sensing Methods: A Review." *Fisheries Research* 49: 1–20. doi:10.1016/S0165-7836(00)00201-0.

Sørensen, K., E. Aas, and J. Høkedal. 2007. "Validation of MERIS Water Products and Bio-Optical Relationships in the Skagerrak." *International Journal of Remote Sensing* 28: 555–568. doi:10.1080/01431160600815566.

Thuillier, G., M. Hersé, D. Labs, T. Foujols, W. Peeterman, D. Gillotay, P. C. Simon, and H. Mandel. 2003. "The Solar Spectral Irradiance from 200 to 2400 nm as Measured by the SOLSPEC Spectrometer from the ATLAS and EURECA Missions." *Solar Physics* 214: 1–22. doi:10.1023/A:1024048429145.

Werdell, P. J., and S. W. Bailey. 2005. "An Improved In-Situ Bio-Optical Data Set for Ocean Color Algorithm Development and Satellite Data Product Validation." *Remote Sensing of Environment* 98 (1): 122–140. doi:10.1016/j.rse.2005.07.001.

Zibordi, G., J.-F. Berthon, J. P. Doyle, S. Grossi, D. van der Linde, C. Targa, and L. Alberotanza. 2002. *Coastal Atmosphere and Sea Time Series (CoASTS), Part 1: A Tower-Based Long-Term Measurement Program.* NASA Technical Memorandum 2002–206892, Vol. 19. Greenbelt, MD: NASA Goddard Space Flight Center.

Zibordi, G., J.-F. Berthon, F. Mélin, D. D'Alimonte, and S. Kaitala. 2009. "Validation of Satellite Ocean Color Primary Products at Optically Complex Coastal Sites: Northern Adriatic Sea, Northern Baltic Proper and Gulf of Finland." *Remote Sensing of Environment* 113: 2574–2591. doi:10.1016/j.rse.2009.07.013.

Zibordi, G., F. Mélin, and J.-F. Berthon. 2006. "Comparison of SeaWiFS, MODIS and MERIS Radiometric Products at a Coastal Site." *Geophysical Research Letters* 33: L06617. doi:10.1029/2006GL025778.

Zibordi, G., F. Mélin, J.-F. Berthon, and E. Canuti. 2013. "Assessment of MERIS Ocean Color Data Products for European Seas." *Ocean Science* 9: 521–533. doi:10.5194/os-9-521-2013.

Zibordi, G., K. Ruddick, I. Ansko, G. Moore, S. Kratzer, J. Icely, and A. Reinart. 2012. "In Situ Determination of the Remote Sensing Reflectance: An Inter-Comparison." *Ocean Science* 8: 567–586. doi:10.5194/os-8-567-2012.